33RD INTERNATIONAL COSMIC RAY CONFERENCE, RIO DE JANEIRO 2013
THE ASTROPARTICLE PHYSICS CONFERENCE

Under-cutoff proton fluxes measured by the PAMELA experiment

A. BRUNO[1] FOR THE PAMELA COLLABORATION

[1] *INFN, Sezione di Bari, I-70126 Bari, Italy.*

alessandro.bruno@ba.infn.it

Abstract: We present a precise measurement of the under-cutoff proton fluxes with kinetic energy >70 MeV performed by the PAMELA mission at low Earth orbit (350-610 km). The analyzed proton sample was classified into three categories: stably-trapped protons from the inner radiation belt; quasi-trapped protons near the magnetic equator, inside and below the inner belt; and un-trapped protons spreading over all geomagnetic latitudes, including the penumbra region. The properties of the different magnetospheric populations were investigated in detail, including locations, energy spectra and pitch angle distributions. PAMELA results significantly improve the description of the low altitude radiation environment and can be used to validate various existing models, providing information on the trapping and interaction processes in the geomagnetic field, and also enhance the knowledge of re-entrant albedo proton fluxes in the magnetosphere, including the penumbra region around the local geomagnetic cutoff.

Keywords: satellite experiments, cosmic rays, radiation belts, trapped protons, albedo protons.

1 Introduction

The radiation environment in Earth's vicinity and, in particular, the Van Allen belts, constitute a well-known hazard for the space missions, involving serious damages to both human health and the spacecraft electronics. These zones are in fact characterized by an intense flux of energetic charged particles, experiencing long-term magnetic trapping. Specifically, the inner belt is mainly populated by protons, mostly originated by the decay of albedo neutrons according to the CRAND mechanism [1, 2]. The standard description of such a environment is still provided by the NASA AP8 semi-empirical model [3], based on data from a series of satellite experiments in the 1960s and early 1970s. Two versions of the model were developed: the former for solar maximum, the latter for solar minimum conditions. Despite of recent improvements [4, 5, 6, 7], the modeling of the low altitude environment is still uncomplete, with largest uncertainties concerning the high energy (>50 MeV) fluxes in the inner zone and the South Atlantic Anomaly (SAA), where the inner belt makes its closest approach to the Earth's surface.

In addition, the radiation measured in the magnetosphere includes populations of re-entrant albedo protons, which have limited lifetime and less intense fluxes [8, 9, 10, 11]. Their description is considerably more complicated due to the interaction with the atmosphere combined with the asymmetry of the geomagnetic field with respect to the geocentric frame[1].

New accurate measurements of the charged cosmic-ray radiation at low Earth orbits have been performed by the PAMELA experiment [12, 13, 14]. Here we present the measurement of the proton fluxes below and around the geomagnetic cutoff.

2 Data analysis

PAMELA is a satellite-based experiment designed for a precise measurement of the charged cosmic radiation in the kinetic energy range from some tens of MeV up to several hundreds of GeV [12]. Details about the apparatus and its performances can be found elsewhere (e.g. [15, 16]). The Resurs-DK1 satellite, which hosts the apparatus, has a semi-polar (70 deg inclination) and elliptical ($350\div610$ km altitude) orbit. The spacecraft is 3-axis stabilized. The orientation is calculated by an onboard processor with an accuracy better than 1 deg which, together with the good angular resolution (<2 deg) of PAMELA, allows particle direction to be accurately measured.

2.1 Data set

The analyzed data set includes protons acquired by PAMELA between July 2006 and September 2009. In order to account for the time variations of PAMELA detector performances, the data sample was dividend into 5 subsets of about 244 days, in relation to the spacecraft orbit precession. The last bin also comprises a few data from the successive (incomplete) period. Measured rigidities were corrected for the energy loss in the apparatus with MonteCarlo simulations. The initial considered sample conservatively included downward-going protons with rigidities lower than $30/L^{-2}$ GV, where L is the McIlwain's parameter [17], in order to investigate, besides of populations well below the geomagnetic cutoff, also particles from the penumbra region, where particles of both cosmic and atmospheric origin are present. McIlwain's coordinates (B, B_{eq}, L) were calculated on an event-by-event basis using the IGRF-05 model [18].

2.2 Particle classification

The trajectories of all selected protons were reconstructed in the Earth's magnetosphere using a trajectory tracing program [19, 20]. They were propagated back and forth from the measurement location, and followed until one of three conditions was satisfied:

1. they reached the Earth's surface;

1. The Earth's magnetic dipole axis is tilted by $\sim$10 deg from the terrestrial rotational axis, and its center is offset by $\sim$500 km from the Earth's core.

2. they reached a radial distance of 25 R_E, where R_E=6371.2 km is the Earth's radius;

3. they performed several revolutions around the Earth.

Events satisfying condition 2 (galactic protons) were excluded from the analysis. The rest of the sample was analyzed according to the adiabatic theory of particle motion in the geomagnetic field: for each event, the numbers of gyrations, bounces and drifts were evaluated to estimate corresponding frequencies and check trajectory behaviors. In order to account for the absorbing atmosphere, only particle paths above an altitude of 40 km were considered.

Then the proton sample was classified into 3 categories:

- protons satisfying the condition 3 without intercepting the absorbing atmosphere (40 km), were identified as "Stably-Trapped" (ST). Their trajectories were verified to satisfy the adiabatic conditions, in particular the hierarchy of temporal scales: $\omega_{bounce}/\omega_{gyro} \leq K_1$ and $\omega_{drift}/\omega_{bounce} \leq K_2$, where ω_{gyro}, ω_{bounce} and ω_{drift} are the frequencies associated to the gyration, the bouncing and the drift motion, respectively; K_1 and K_2 values are of the order of ~ 0.1. Their distribution is limited to the SAA at PAMELA altitudes.

- Protons with similar trajectories, but originated and re-absorbed by the atmosphere during a time larger than a bounce period were considered as "Quasi-Trapped" (QT). They are concentrated in the near equatorial region.

- The rest of the sample was considered as "Un-Trapped" (UT), including both a short lived component spreading over all latitudes, together with a long lived component concentrating in the region corresponding to rigidities $R \geq 4/L^2$ GV, and characterized by complex trajectories of non-adiabatic type: such protons can perform several drift cycles (up a few hundreds) and reach large distances from the Earth before being absorbed by the atmosphere.

The lifetime of the QT and UT populations was estimated from the tracing procedure, as the time between the particle origin (traced backward) and its subsequent absorption (traced forward) in the atmosphere (i.e. the tracing time τ). Results are reported in figure 1, where the lifetime for the measured sample is shown as a function of kinetic energy for both low (Λ<35 deg) and middle-high (Λ>35 deg) latitudes (top and bottom panel, respectively). QT protons lifetime is typically shorter than a drift period ($\tau \sim 0.3 \div 30$ s), while the upper bands (τ up to ~ 2 min) correspond to QT particles performing more than a revolution around the Earth. Since the QT proton lifetime is of the order of a half drift period, which scales with $\sim 1/\gamma\beta^2$ [21], lifetime and energy have an approximately inverse proportional relation. Differently, the UT proton lifetime at low latitudes ranges from some fraction of *s* to a few *s* and it is shorter than the typical bounce period, which scales with $1/\beta$, resulting in a weaker dependency on energy. In particular, their distribution is given by two superimposed bands, corresponding to particles crossing the magnetic equator once and twice, respectively. Indeed, a population of very-short-lived (< 30 *ms*) equatorially mirroring protons emerges at high energies ($0.8 \div 8$ GeV), with a tracing time increasing with energy: because of the large gyro-radius with respect to the magnetic field curvature, such

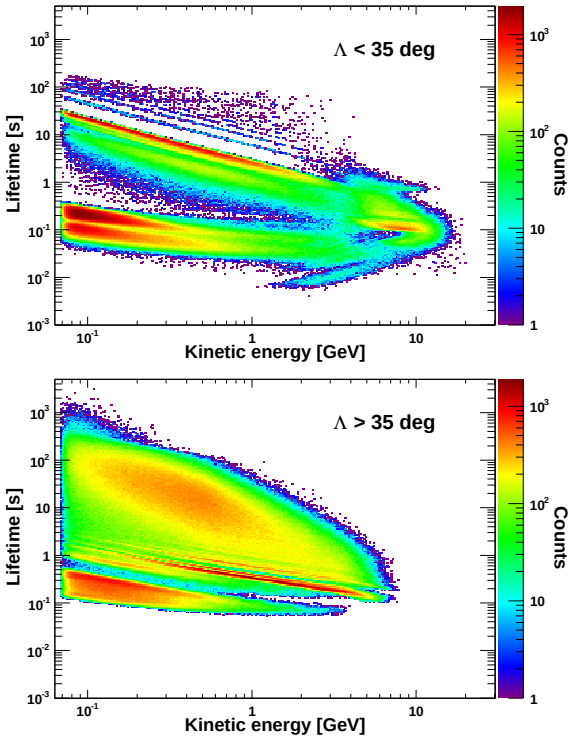

Figure 1: Count distributions as a function of the tracing time and of kinetic energy, for both low (Λ<35 deg, top panel) and high (Λ>35 deg, bottom panel) latitudes.

particles have no stable bounce motion ($\omega_{bounce} \sim \omega_{gyro}$, large ω_{drift} values). Finally, the long-lived (τ up to 10^3 s) UT component concentrates at higher latitudes, resulting in a much broader distribution.

2.3 Flux calculation

Since fluxes inside and near the SAA are significantly anisotropic, the gathering power of the apparatus [22] depends on the spacecraft orientation with respect to the geomagnetic field. Consequently, a PAMELA effective area (cm^2) was evaluated as a function of particle energy E, local pitch angle α and orientation Ψ:

$$H(E,\alpha,\Psi) = \frac{1}{2\pi}\int_0^{2\pi} d\beta\,[A(E,\theta,\phi)\cdot sin\alpha\cdot cos\theta] \quad (1)$$

where β is the gyro-phase angle, and θ=$\theta(\alpha,\beta,\Psi)$ and ϕ=$\phi(\alpha,\beta,\Psi)$ are respectively the zenith and the azimuth angle describing particle direction in the PAMELA frame[2], and $A(E,\theta,\phi)$ is the apparatus response function. The effective area was evaluated with Monte Carlo integration methods [22], averaging over β. The calculation was performed by varying the local pitch α in steps of 1 deg in the range $0 \div 180$ deg. The satellite orientation $\Psi = (\theta_\Psi, \phi_\Psi)$, where θ_Ψ and ϕ_Ψ denote respectively the zenith and azimuth angles. of geomagnetic field direction in the PAMELA reference frame, was varied in steps of $\Delta\theta_\Psi$,$\Delta\phi_\Psi$=1 deg, over the ranges of possible values ($0 \leq$

2. The PAMELA frame has the origin in the center of the spectrometer cavity; the Z axis is directed along the main axis of the apparatus, toward incoming particles; the Y axis is directed opposite to the main direction of the magnetic field inside the spectrometer; the X axis completes a right-handed system.

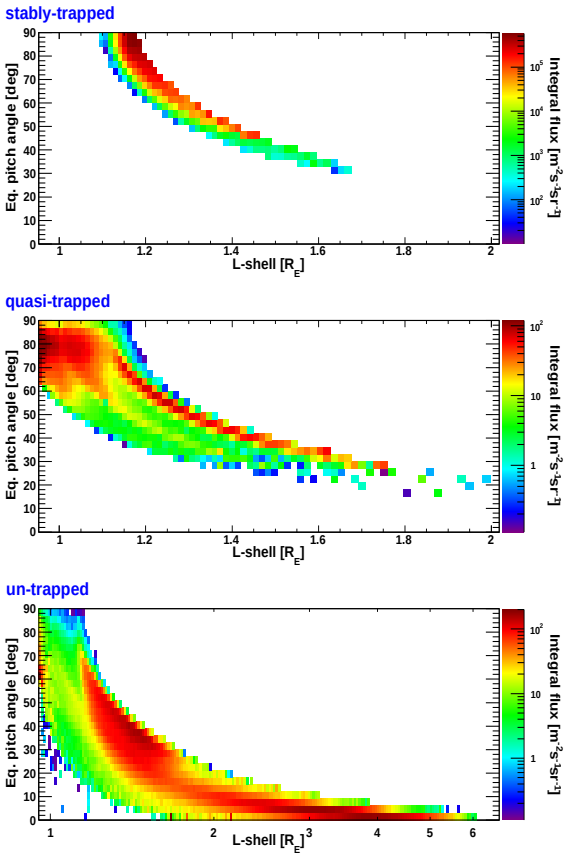

Figure 2: Proton integral fluxes ($m^{-2}s^{-1}sr^{-1}$, $E > 70$ MeV) as a function of equatorial pitch angle and McIlwain's L-shell, for the different under-cutoff populations.

ϕ_Ψ <360 deg, 0≤ θ_Ψ <180 deg). The dependency of the effective area on particle rigidity R was studied by estimating $H(E,\alpha,\Psi)$ in 40 logarithmic bins (R = 0.35÷30 GV).

Finally, in order to account for effects due to the large particle gyro-radius (up to several hundreds of km), fluxes were evaluated by shifting measured protons (L, B, B_{eq}) to corresponding guiding center positions (L_{gc}, B_{gc}, $B_{eq,gc}$).

3 Results

Directional integral fluxes ($m^{-2}s^{-1}sr^{-1}$, $E > 70$ MeV) of under-cutoff protons as a function of equatorial pitch angle α_{eq} and McIlwain's L-shell are reported in figure 2. In particular, the top panel reports results for ST protons. Since PAMELA orbit reaches the equator only for L-shell values up to ∼1.18 R_E, the coverage of data in (L,α_{eq}) is incomplete, so that distribution of stably-trapped is a strip of limited width parallel to the drift loss cone[3] PAMELA trapped fluxes were compared with predictions from the AP8-min [3] and SAMPEX/PET PSB97 [6] semi-empirical models. As example, the energy spectrum evaluated at L=1.16 R_E and α_{eq}=73.5 deg is reported in figure 3.

As a consequence of the lack of symmetry of the geomagnetic field with respect to the Earth's rotational axis, QT and UT fluxes depend on longitude as well, so 2D maps do not adequately describe such populations: in fact, resulting distributions are given by a convolution of fluxes measured in regions characterized by different bounce loss cone values, from the SAA (highest L-shells), where the

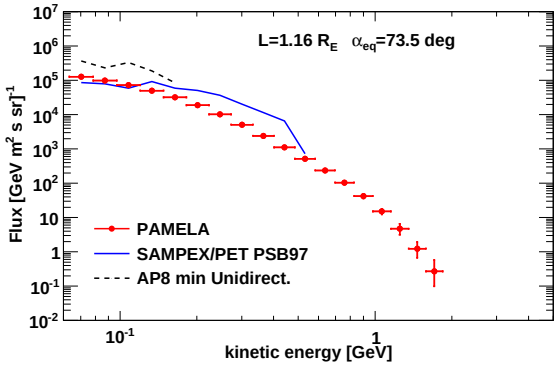

Figure 3: Stably-trapped proton energy spectrum ($GeV^{-1}m^{-2}s^{-1}sr^{-1}$) evaluated at L=1.16 R_E and α_{eq}=73.5 deg. Predictions from AP8-min (black dotted line) and SAMPEX/PET PSB97 (blue solid line) models are also reported for a comparison. Model calculations from the SPENVIS on-line system [23].

geomagnetic field is minimum, to the side of the Earth opposite to the SAA (lowest L-shells), where the geomagnetic field has a local maximum. QT flux intensities are 2÷3 orders of magnitude lower with respect to ST fluxes, and concentrate in the near equatorial region ($L < 2$ R_E). Their fluxes result to be quite isotropic, except for the SAA, where distributions are similar to those of ST protons. Similar features characterize the UT population, which spreads over all latitudes with a peak of low energy protons in the SAA region, and an additional increase at highest energies and L-shells.

Fluxes were also mapped using the Altitude Adjusted Corrected Geomagnetic (AACGM) coordinates [24], developed to provide a more realistic description of high latitude regions, by accounting for the multipolar geomagnetic field. The energy spectra calculated for different latitude bins are reported in figure 4. They were estimated by averaging over the AACGM longitude range [-60,120] deg in order to exclude the SAA, so results include only QT and UT components. Spectra show some structures at highest energies: in particular, a significant peak is present in the penumbra region, around the geomagnetic cutoff.

Finally, figure 5 shows the integral fluxes of the different populations as a function of geographical coordinates, averaged over the ranges of altitudes and pitch angles covered by PAMELA.

4 Conclusions

PAMELA measurements of energetic (> 70 MeV) under-cutoff proton fluxes at low Earth orbits (350÷610 km) have been presented. The detected sample, corresponding to data acquired by PAMELA between July 2006 and September 2009, was analyzed according to the adiabatic theory of charged particle motion in the geomagnetic field, and classified into three components on the basis of trajectory behaviors in the magnetosphere evaluated with particle tracing techniques.

3. The (bounce) loss cone is given by α_{eq} values along the same field line for which magnetic trapping does not occur. The drift loss cone corresponds to the maximum loss cone along a given drift shell.

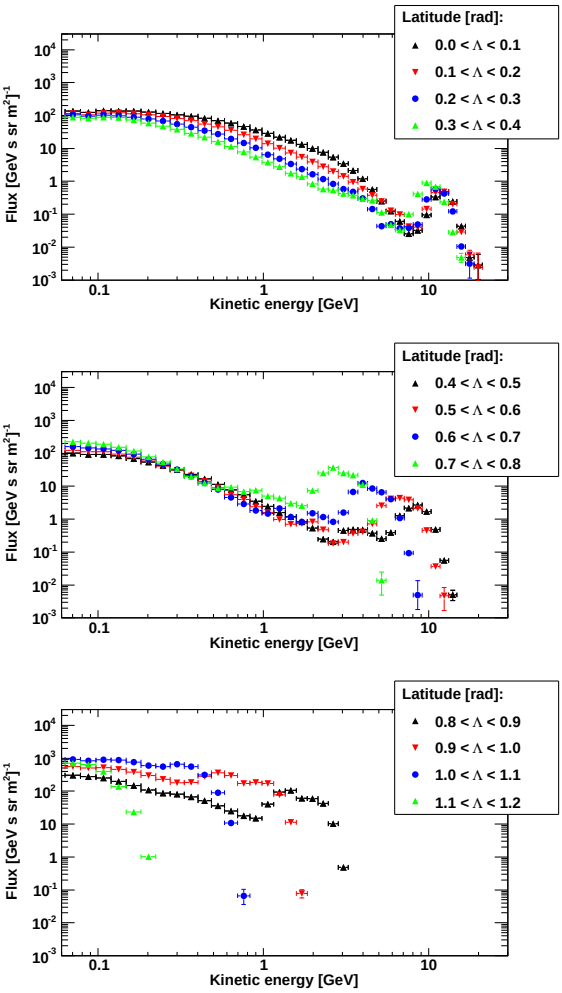

Figure 4: Proton energy spectra ($GeV^{-1}m^{-2}s^{-1}sr^{-1}$) calculated for different AACGM latitudes (see text for details).

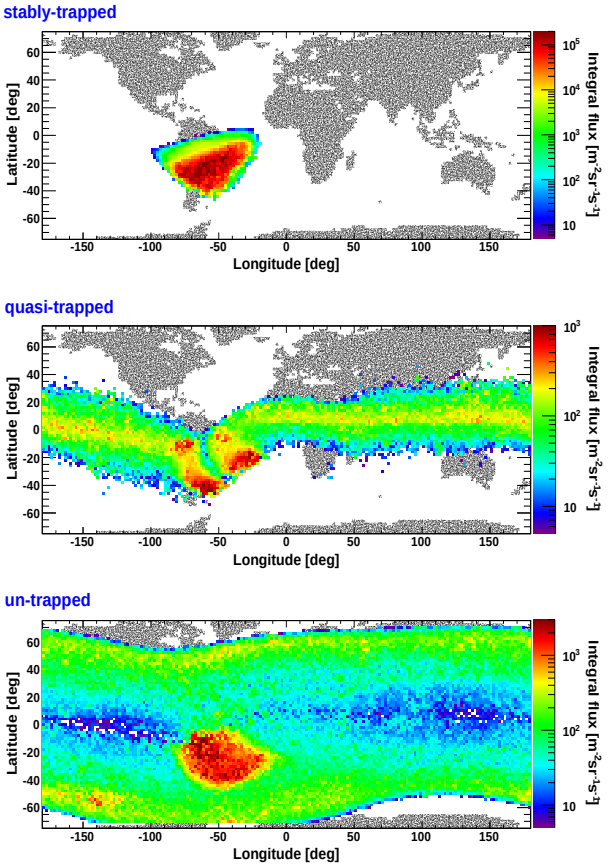

Figure 5: Proton integral fluxes ($m^{-2}s^{-1}sr^{-1}$, $E > 70$ MeV) as a function of geographic longitude and latitude, for the different under-cutoff populations.

PAMELA results extend the observational range for the trapped radiation down to lower L-shells ($\sim 1.05\ R_E$) and up to highest kinetic energies (~ 4 GeV), significantly improving the description of the low altitude radiation environment in regions where models suffer from the largest uncertainties. PAMELA measurements provide important information on the trapping and interaction processes in the geomagnetic field, and also enhance the description of re-entrant albedo protons in different regions of the magnetosphere.

References

[1] S.F. Singer, 1958, Phys. Rev. Lett., 1, 181– 183.
[2] T.A. Farley, & M. Walt, 1971, J. Geophys. Res., 76, 8223– 8240.
[3] D.M. Sawyer, & J.I. Vette, 1976, NSSDC/WDC-A-R&S 76-06.
[4] J.D. Meffert, & M.S. Gussenhoven, 1994, PL-TR-94-2218, Environ. Res. Pap. 1158.
[5] S.L. Huston, & K.A. Pfitzer, 1998, NASA Contract. Rep. NASA/CR-1998-208593.
[6] D. Heynderickx, et al., 1999, IEEE Trans. Nucl. Sci., Vol. 46, pp. 1475-1480.
[7] M.A. Xapsos, et al., 2002, IEEE Trans. Nucl. Sci., 49, 2776–2781.
[8] J. Moritz, 1972, Z. Geophys. 38, 701.
[9] D. Hovestadt, et al., 1972, Phys. Rev. Lett. 28, 1340.
[10] J. Alcaraz, et al., 2000, Phys. Lett. B 472:215-226.
[11] E. Fiandrini, et al., 2004, J. Geophys. Res., 109, 10214.
[12] P. Picozza, et al., 2007, Astropart. Phys., Vol 27, pp. 296-315.
[13] O. Adriani, et al., 2009, J. Geophys. Res., 114, A12218.
[14] O. Adriani, et al., 2011, ApJ 737 L29.
[15] A. Bruno, Ph.D. thesis, University of Bari, Bari, Italy, 2008, http://pamela.roma2.infn.it/.
[16] O. Adriani, et al., Sciencexpress, 3 March 2011.
[17] C. McIlwain, 1966, Space Sci. Rev. 5, 585-589.
[18] S. Maus, et al., 2005, Earth Planets Space, 57 1173-1181.
[19] D.F. Smart, & M.A. Shea, 2000, Final Report, Grant NAG5-8009.
[20] D.F. Smart, & M.A. Shea, 2005, Adv. Space Res., 36, 2012–2020.
[21] M. Walt, 1994, Introduction to Geomagnetically Trapped Radiation, Cambridge Univ. Press., New York.
[22] J.D. Sullivan, 1971, Nucl. Instr. and Meth. 95, 5.
[23] D. Heynderickx, et al., 2002, SAE Technical Paper 2000-01-2415.
[24] W. Heres & N.A. Bonito, 2007, Scientific Report AFRL-RV-HA-TR-2007-1190.